

Study of HERA ep Data at Low Q^2 and Low x_{Bj} and the Need for Higher-Twist Corrections to Standard pQCD Fits

I. Abt^a, A.M. Cooper-Sarkar^b, B. Foster^{b,c,d}, V. Myronenko^d,
K. Wichmann^d, M. Wing^e

^a Max-Planck-Institut für Physik, Werner-Heisenberg-Institut, München, Germany

^b Physics Department, University of Oxford, Oxford, U.K.

^c Hamburg University, I. Institute of Exp. Physics, Hamburg, Germany

^d Deutsches Elektronen Synchrotron DESY, Hamburg, Germany

^e University College London, U.K.

Abstract

A detailed comparison of HERA data at low Bjorken- x and low four-momentum-transfer squared, Q^2 , with predictions based on $\ln Q^2$ evolution (DGLAP) in perturbative Quantum Chromo Dynamics suggests inadequacies of this framework. The standard DGLAP evolution was augmented by including an additional higher-twist term in the description of the longitudinal structure function, F_L . This additional term, $F_L A_L^{\text{HT}}/Q^2$, improves the description of the reduced cross sections significantly. The resulting predictions for F_L suggest that further corrections are required for Q^2 less than about 2 GeV^2 .

1 Introduction

Analyses of HERA and other DIS data are generally performed within the perturbative regime of Quantum Chromo Dynamics (QCD), [1] i.e. with Q^2 , the four-momentum-transfer squared, sufficiently above 1 GeV^2 . The HERA data extend towards Q^2 and x_{Bj} values, where x_{Bj} is the Bjorken scaling variable, where the longitudinal structure function, F_L , becomes significant. Previous HERA results [2,3] suggest that QCD continues to give a good description of the data down to surprisingly low values of Q^2 . This gives the possibility of not only establishing the limit below which QCD no longer describes the data, but also of investigating modifications to the standard Dokshitzer–Gribov–Lipatov–Altarelli–Parisi (DGLAP) [4–8] evolution that have been proposed in the literature, for example $\ln(1/x)$ resummations, as introduced by Balitsky–Fadin–Kuraev–Lipatov [9], or saturation. The key variable is x , the fraction of the proton momentum carried by the parton, which is identical to x_{Bj} in the quark–parton model. Saturation is expected to occur when the density of gluons becomes so large that the standard increase in gluon density as x falls is flattened off by gluon–gluon interactions and recombination. Such effects can be described by non-linear evolution equations including higher-twist corrections at low x , visualised as gluon ladders with recombining gluons [10,11]. An earlier analysis of HERA-I data [12] had shown some discrepancies with conventional DGLAP evolution at low Q^2 and low x . This is now investigated using the final combination of HERA inclusive cross sections.

This combination of HERA reduced cross sections for Neutral Current (NC) and Charged Current (CC) $e^\pm p$ scattering measured by the H1 and ZEUS collaborations was recently published [3] together with a QCD analysis based solely on the DGLAP formalism, which produced a set of parton distribution functions (PDFs) called HERAPDF2.0. In this analysis, it was noted that the predictions from the PDFs of HERAPDF2.0 were not able to describe the NC data very well at low Q^2 , below $Q^2 \approx 10 \text{ GeV}^2$, both at NLO and NNLO. This was confirmed within the framework of the NNPDF global analysis [13].

The reduced NC deep inelastic $e^\pm p$ scattering cross sections are given by a linear combination of structure functions which depends on the PDFs. At low Q^2 , where virtual photon exchange is dominant, the reduced cross sections for $e^\pm p$ scattering are equal and may be expressed in terms of the structure functions F_2 and F_L as

$$\sigma_{r,\text{NC}}^\pm = \frac{d^2\sigma_{\text{NC}}^{e^\pm p}}{dx dQ^2} \cdot \frac{Q^4 x_{\text{Bj}}}{2\pi\alpha^2 Y_\pm} = F_2 - \frac{y^2}{Y_\pm} F_L, \quad (1)$$

where the fine-structure constant, α , the photon propagator and a helicity factor are absorbed in the definitions of $\sigma_{r,\text{NC}}^\pm$ and $Y_\pm = 1 \pm (1-y)^2$. In particular, the predictions of HERAPDF2.0 were not able to describe the turn-over of the neutral current reduced cross section at low x_{Bj} and low Q^2 due to the contribution from F_L , which is directly connected to the gluon PDF [14].

The analysis presented here focuses on a simple *ansatz* to add higher-twist terms to the DGLAP-based evolution. The expectation is that such terms are important for F_L , but not for the structure function F_2 , because in the case of F_2 longitudinal and transverse contributions cancel [10]. New sets of PDFs were extracted at next-to-leading order (NLO) and next-to-next-to-leading order (NNLO). These PDFs are called the HHT PDFs and the corresponding analyses are called the HHT analyses, for ease of reference. The predictions from these analyses are compared to the reduced HERA cross sections at low Q^2 and low x_{Bj} . The predictions of HHT

and HERAPDF2.0 for F_L are compared to measurements published separately by the H1 [15] and ZEUS [16] collaborations.

2 The HERA Data and HERAPDF2.0

The HERA data on neutral current and charged current e^+p and e^-p inclusive cross sections as combined by the H1 and ZEUS collaborations [3] were used as the input to the analysis presented here. Their kinematic range spans six orders of magnitude in x_{Bj} and Q^2 , but only four orders of magnitude are usable for pQCD fits, for which Q_{\min}^2 must be above 1 GeV². The range in x_{Bj} is automatically reduced when low- Q^2 data are excluded, because, at HERA, low x_{Bj} also implies low Q^2 .

The data were previously used to extract the HERAPDF2.0 [3] set of PDFs. While the description of the data by the predictions of HERAPDF2.0 is quite good, the overall χ^2 /(number of degrees of freedom, ndof) values of the various fits were around 1.2 [3]. It was observed that these values could be reduced if Q_{\min}^2 , the smallest Q^2 of the data used in the fits, was increased from 3.5 GeV² to 10 GeV². However, this substantially worsened the predictions for the low- Q^2 and low- x_{Bj} regime, which were already not particularly good either at NLO or NNLO for the standard fits with $Q_{\min}^2 = 3.5$ GeV². Neither did NNLO fits show any improvement over NLO ones.

Most of the HERA data were taken with a centre-of-mass energy, \sqrt{s} , of 318 GeV. However, NC e^+p data are available also for lower \sqrt{s} , such that different values of the inelasticity y are accessed at the same x_{Bj} and Q^2 , since $y = sx/Q^2$. This provides direct information on F_L . Although results on F_L were published separately by the H1 and ZEUS collaborations, the data on which the results were based were combined and were included in the data set used for the HHT analysis.

3 QCD Analysis Including Higher-Twist Effects

The introduction of higher-twist terms is one possible way to extend the DGLAP framework. Higher-twist effects have a $1/Q^{2n}$ dependence and are thus important at low Q^2 . Such terms have been introduced by previous authors, but usually in the context of higher-twist effects which are important at high x [17]. In the present paper we investigate low- x higher-twist effects since, for the kinematics of HERA, low Q^2 is only accessed at low x_{Bj} . Motyka *et al* [18] have also considered higher-twist effects at low x but in the context of diffractive data. In the present study we concentrate on inclusive data. The leading-twist perturbative QCD forms of the structure functions F_2 and F_L were augmented by simple twist-4 terms

$$F_2^{\text{HT}} = F_2^{\text{DGLAP}} (1 + A_2^{\text{HT}}/Q^2), \quad (2)$$

$$F_L^{\text{HT}} = F_L^{\text{DGLAP}} (1 + A_L^{\text{HT}}/Q^2), \quad (3)$$

where A_2^{HT} and A_L^{HT} are free parameters in the fits.

The ZEUSfitter package ¹ was used for the analysis presented here. The results were cross-checked with the HERAFitter [20] package. Except for the addition of the higher-twist term, the fits called HHT were set up exactly as the HERAPDF2.0 fits. In particular the heavy-flavour scheme used was the RTOPT scheme [21–23] and the minimum value of Q^2 for data entering the fit was $Q_{\min}^2 = 3.5 \text{ GeV}^2$. The value of $Q_{\min}^2 = 3.5 \text{ GeV}^2$ was chosen as it was assumed that non-perturbative effects would only appear at Q^2 below this value. Other groups work with even lower Q_{\min}^2 , for example MSTW/MMHT [24,25] use $Q_{\min}^2 = 2.0 \text{ GeV}^2$. A higher-twist term as introduced in Eq. 3 was tested by MMHT and found to improve the χ^2 values of their fits [26] to HERA and other data. In the present paper the effects of such a higher-twist term on the predictions for F_2 and $\sigma_{r,\text{NC}}^\pm$ are explored in more detail, using an analysis focussing on HERA data.

The PDFs for HHT were parameterised at the starting scale $\mu_{f_0}^2 = 1.9 \text{ GeV}^2$. The gluon PDF, directly connected to F_L^{DGLAP} , was parameterised as

$$xg(x) = A_g x^{B_g} (1-x)^{C_g} - A'_g x^{B'_g} (1-x)^{C'_g}, \quad (4)$$

where A_g, B_g, C_g and A'_g, B'_g are free parameters and C'_g was set to 25 [24]. The A'_g was added to make the parameterisation more flexible at low x . It could lead to a negative gluon density at low x , even at scales above $\mu_{f_0}^2$. However, this was neither observed for HERAPDF2.0 nor for the analysis presented here.

The HHT fits were performed at NNLO and NLO, including the higher-twist term for F_2 only, F_L only and both F_2 and F_L . The uncertainties from the fits are taken as experimental uncertainties and are the only uncertainties considered throughout the paper. The introduction of A_L^{HT} was found to reduce the χ^2/ndof of the fit significantly, both at NLO and at NNLO. However, adding A_2^{HT} had no significant effect. For the NNLO fit, it only reduced the χ^2/ndof from 1363/1131 to 1357/1130 and the corresponding value of A_2^{HT} was consistent with zero, i.e. $A_2^{\text{HT}} = 0.12 \pm 0.07 \text{ GeV}^2$. Similar values for A_2^{HT} were obtained when A_2^{HT} and A_L^{HT} were included simultaneously. Therefore, all HHT fits presented in this paper include only the A_L^{HT} term. This agrees with predictions [10] that higher-twist terms would be observable in F_L but not in F_2 because the contributions from longitudinally and transversely polarised photons would cancel for F_2 .

The HHT PDFs, xd_v and xu_v for the valence quarks and xS for the sea quarks together with xg , are shown in Fig. 1. The PDFs of HHT are very similar to the PDFs of HERAPDF2.0, even though the values of A_L^{HT} extracted are quite high: $A_L^{\text{HT}} = 5.5 \pm 0.6 \text{ GeV}^2$ from the NNLO and $A_L^{\text{HT}} = 4.2 \pm 0.7 \text{ GeV}^2$ from the NLO fit. The PDFs of HHT remain very similar to those of HERAPDF2.0 when they are evolved in Q^2 up to the scale of the LHC, across the kinematic reach of x_{Bj} of the ATLAS, CMS and LHCb experiments. Thus the need for higher-twist terms at low Q^2 has no effect on LHC physics.

The χ^2/ndof for HHT NNLO is 1316/1130 and for HHT NLO 1329/1130. This may be compared to the HERAPDF2.0 χ^2/ndof values of 1363/1131 for the NNLO and 1356/1131 for the NLO fit. This represents an improvement of $\Delta\chi^2 = -27$ for NLO and an even more significant $\Delta\chi^2 = -47$ at NNLO. Table 1 details the main contributions to this reduction of χ^2 . The HHT fit at NNLO has a lower χ^2 than the fit at NLO. This is a reversal of the situation for HERAPDF2.0. Table 1 also lists the partial χ^2/ndp values for the high-precision NC e^+p

¹The package was recently also used in a combined electroweak and QCD analysis of HERA data [19].

data with $\sqrt{s} = 318 \text{ GeV}^2$. In addition, the χ^2/ndp values for the data points below $Q_{\min}^2 = 3.5 \text{ GeV}^2$ down to 2.0 GeV^2 are listed. These χ^2 values provide an evaluation of the quality of the predictions below Q_{\min}^2 and quantify that the extrapolation of HHT NNLO describes these data better than the extrapolation of HERAPDF2.0, while the description at NLO does not improve.

The positive higher-twist terms preferred by the HHT fits imply that F_L is larger than determined in the HERAPDF2.0 fits. Since the structure function F_L is directly related to the gluon distribution at low x , at $\mathcal{O}(\alpha_s)$, it might be expected that a larger F_L implies at larger low- x gluon. However, this ignores the role of higher-order matrix elements. In fact, the NNLO gluon distribution exhibits a turn-over at low x and Q^2 . This comes from the substantial A'_g term which the HHT NNLO fit requires even in the presence of the large higher-twist term. To investigate this a gluon parametrisation of the form $xg(x) = A_g x^{B_g} (1-x)^{C_g} (1 + D_g x)$ was also tested at both NLO and NNLO. This form is called the alternative gluon or AG form of the parametrisation and it ensures that the gluon distribution is always positive definite for $Q^2 \geq \mu_{f_0}^2$. The AG fits and the fits using the form of Eq. 4 are very similar at NLO. In contrast, the AG parameterisation at NNLO results in much higher χ^2/ndof values, 1389/1131 for HERAPDF2.0 and 1350/1130 for HHT. At NNLO the data favour a strong gluon turn-over whereas AG, by construction, does not allow this. The AG parameterisation is clearly not suited for fits at NNLO.

The validity of the assumption that perturbation theory is applicable in the kinematic regime of the fits is tested by the dependence of the quality of the fits, as represented by χ^2/ndof , on the value of Q_{\min}^2 . The value of χ^2/ndof should ideally not depend strongly on Q_{\min}^2 . The dependence of χ^2/ndof on Q_{\min}^2 for HHT and HERAPDF2.0 is shown in Fig. 2 for both NNLO and NLO. The values drop steadily until $Q_{\min}^2 \approx 10 \text{ GeV}^2$, when the χ^2/ndof becomes similar for HHT and HERAPDF2.0. The effect of the higher-twist term is, as expected, confined to the low- Q^2 region. The HHT fits show a slower rise in χ^2 as Q_{\min}^2 is reduced.

The fits with $Q_{\min}^2 = 2.0 \text{ GeV}^2$ close to the starting scale $\mu_{f_0}^2 = 1.9 \text{ GeV}^2$ were studied in more detail. The relevant χ^2 values are listed in Table 2. The PDF and especially the higher-twist parameters of HHT NNLO do not change much when Q_{\min}^2 is lowered from 3.5 GeV^2 to 2.0 GeV^2 . The partial χ^2/ndp for the NC e^+p data with $\sqrt{s} = 318 \text{ GeV}$ increases from 1.12 to 1.14, but the partial χ^2/ndp drops from 1.28 to 1.04 for the 25 points in the range $2.0 \leq Q^2 < 3.5 \text{ GeV}^2$.

Refitting with lower Q_{\min}^2 has a stronger effect at NLO than at NNLO, but again, the higher-twist term is basically unchanged. The results at NLO are, as before, not strongly dependent on the details of the gluon distribution. This can be seen when refitting with HHT NLO AG, which yields almost the same result as HHT NLO.

4 Heavy-Flavour Schemes

The influence of the heavy-flavour scheme was already discussed in the context of HERAPDF2.0 [3]. To study the effect on this analysis, the HERAFitter [20] package was used to replace the default RTOPT scheme with the FONLL scheme [27,28]. The resulting dependence of χ^2 on Q_{\min}^2 is shown in Fig. 3, together with the values from the standard fits.

In the FONLL scheme, the HHT NNLO fit has a substantially improved χ^2/ndof for low Q_{\min}^2 compared to HERAPDF2.0, just as for the standard HHT NNLO fit with RTOPT. The value of the higher-twist parameter $A_L^{\text{HT}} = 6.0 \pm 0.7 \text{ GeV}^2$ is also similar. However, the HHT NLO FONLL fit has only a marginally improved χ^2/ndof for low Q^2 as compared to HERAPDF2.0 and a small value of A_L^{HT} , i.e. $A_L^{\text{HT}} = 1.2 \pm 0.6 \text{ GeV}^2$. This is probably associated with the order of α_s at which F_L is evaluated in these different heavy-flavour schemes. RTOPT at NLO calculates F_L to $\mathcal{O}(\alpha_s^2)$ and RTOPT at NNLO calculates F_L to $\mathcal{O}(\alpha_s^3)$. FONLL at NLO calculates F_L to $\mathcal{O}(\alpha_s)$ and FONLL at NNLO calculates F_L to $\mathcal{O}(\alpha_s^2)$. Only calculating F_L to $\mathcal{O}(\alpha_s)$ results in a relatively large F_L , which can reduce the need for a higher-twist term. However, as soon as F_L is calculated to $\mathcal{O}(\alpha_s^2)$ or higher, a higher-twist term is required. The best fit achieved for HHT NNLO is with the RTOPT scheme.

5 Reduced Cross Sections

A comparison of the predictions of HHT and HERAPDF2.0 with $Q_{\min}^2 = 3.5 \text{ GeV}^2$ to the measured reduced NC e^+p cross sections is shown at NNLO in Fig. 4 and at NLO in Fig. 5. In all cases, the predictions are extrapolated down to $Q^2 = 2.0 \text{ GeV}^2$; HHT clearly describes this low- Q^2 , low- x_{Bj} data better. This was already indicated by the χ^2/ndf values in Table 1, where the χ^2/ndf for the data points with $2.0 \leq Q^2 < 3.5 \text{ GeV}^2$ are listed separately. The HHT NNLO predictions are clearly preferred as they describe the turn-over of the data towards low x_{Bj} quite well. This turn-over region at low x_{Bj} is not well described by the predictions from HERAPDF2.0.

The predictions of the HHT NNLO and HHT NLO with $Q_{\min}^2 = 2.0 \text{ GeV}^2$ are shown in Fig. 6. The data are well described at NNLO, even better than for the standard HHT NNLO with $Q_{\min}^2 = 3.5 \text{ GeV}^2$. The effect of the lower Q_{\min}^2 is stronger at NLO, where the turn-over is better described.

The HHT NNLO predictions even describe the data down to $Q^2 = 1.2 \text{ GeV}^2$ quite well, as can be seen in Fig. 7. This is especially true for HHT NNLO with $Q_{\min}^2 = 2.0 \text{ GeV}^2$. At $Q^2 = 1.5 \text{ GeV}^2$, the turn-over is very well described. At $Q^2 = 1.2 \text{ GeV}^2$, the predicted turn-over is somewhat shifted towards higher x_{Bj} . However, it is remarkable how well these data below the starting scale of the evolution are described, illustrating once again the apparent ability of a perturbative QCD *ansatz* to describe the data to surprisingly low Q^2 .

6 The Structure Functions F_2 and F_L

Values of the structure function F_2 are extracted from the data as

$$F_2^{\text{extracted}} = F_2^{\text{predicted}} \frac{\sigma_r^{\text{measured}}}{\sigma_r^{\text{predicted}}} . \quad (5)$$

The values of $F_2^{\text{extracted}}$ together with $F_2^{\text{predicted}}$ are shown in Figs. 8 and 9 for HHT and HERAPDF2.0 at NNLO and NLO, respectively. At NNLO, the HHT predictions and extractions agree well down to $Q^2 = 2.0 \text{ GeV}^2$. Since A_L^{HT} is substantial, the predictions from HHT for

F_L are larger than from HERAPDF2.0 at low Q^2 . Since $\sigma_r = F_2 - F_L y^2/Y_+$, see Eq. 1, this results also in larger predictions for F_2 and in larger values of $F_2^{\text{extracted}}$. The agreement between prediction and extraction is better for HHT. This confirms that the F_L from HERAPDF2.0 is not large enough. The predicted and the extracted values also agree better for HHT at NLO, but the NLO fit is not as good as the NNLO fit below around $Q^2 = 4.5 \text{ GeV}^2$.

In Fig. 10, $F_2^{\text{predicted}}$ and $F_2^{\text{extracted}}$ are shown for HHT NNLO and NLO with $Q_{\text{min}}^2 = 2.0 \text{ GeV}^2$. The situation for the NNLO fit looks very similar to the fit with $Q_{\text{min}}^2 = 3.5 \text{ GeV}^2$. The description of the data by the predictions of the NLO fit is improved at low x_{Bj} and low Q^2 . However, $F_2^{\text{extracted}}$ still shows a tendency to turn-over. This confirms the findings of the comparisons with the reduced cross-section data that HHT NNLO is better suited to describe the data than HHT NLO.

The H1 and ZEUS collaborations published separate measurements of F_L [15,16], using data with lowered \sqrt{s} provided cross sections at different y for identical x_{Bj} and Q^2 . The predictions of HHT and HERAPDF2.0 with $Q_{\text{min}}^2 = 3.5 \text{ GeV}^2$ for F_L at NNLO and NLO are compared to these measurements in Fig. 11. For $Q^2 > Q_{\text{min}}^2$, the shapes of all predicted curves are similar but the predictions of HHT are significantly higher than those from HERAPDF2.0 for Q^2 below 50 GeV^2 . Even though the statistical accuracy of the data is limited, the data mildly favour HHT over HERAPDF2.0 in this regime.

In Fig. 11, extrapolated F_L predictions are shown below $Q_{\text{min}}^2 = 3.5 \text{ GeV}^2$ and even below the starting scale $\mu_{f_0}^2 = 1.9 \text{ GeV}^2$. These predictions have large uncertainties and the accuracy of the data is limited, but it is clear that the upturn of F_L predicted by HHT NNLO is not favoured by the data. This disagreement on F_L is in contrast to the fact that the predictions of HHT NNLO describe the very precise NC e^+p cross sections down to $Q^2 = 1.2 \text{ GeV}^2$ remarkably well, see Fig. 7. Although the higher-twist term is expected to be important for F_L [10], the very large increase of the predicted F_L suggests that some other effect is being absorbed in F_L in the simple *ansatz* used in the current analysis. Since HERA kinematics couples low Q^2 to low x it could be that $\ln(1/x)$ resummation has a role to play here.

Interestingly, HERAPDF2.0 NNLO also predicts a slight upturn of F_L at Q^2 below Q_{min}^2 . This suggests that the upturn in both the HHT and HERAPDF2.0 NNLO analyses is connected to the NNLO coefficient functions, which are large and positive. Similar effects were observed previously [29] for predictions from both pure DGLAP analyses and those including higher-twist terms.

7 Saturation

The operator-product expansion beyond leading twist has diagrams in which two, three or four gluons may be exchanged in the t-channel such that these gluons may be viewed as recombining. This recombination could lead to gluon saturation [11]. The A_L^{HT}/Q^2 -term used in the analysis presented here corresponds to twist-4. Another approach to describe saturation is the colour-dipole picture, which is formulated in the proton rest frame where the incoming photon develops structure over a coherence length proportional to $1/Q^2$ and $1/x_{\text{Bj}}$. Recently, fits to the HERA data were presented [30], which indicate that saturation effects should set in at latest at $x_{\text{Bj}} > 10^{-9}$, but possibly earlier. The data presented here reach down to $x_{\text{Bj}} \approx 10^{-5}$. It is therefore

interesting to see if there is any hint of saturation effects becoming important already in these HERA data.

Phenomenological models of saturation have been treated in the colour-dipole picture. A successful dipole model using the non-linear running-coupling Balitsky-Kovchegov equation [31, 32] has been developed by Albacete *et al.* [33]. However, fits in such a scheme are beyond the scope of the present paper. Instead we compare our data with the predictions of a simple dipole model of saturation [34] by Golec-Biernat and Wüsthoff (GBW), in which the onset of saturation is characterised as the transition from a “soft” to a “hard” scattering regime. This occurs along a “critical line” in the x_{Bj}, Q^2 plane. Fits to early HERA data with low Q^2 and low x_{Bj} indicated that the critical line would be around $x_{\text{Bj}} = 10^{-4}$ at $Q^2 = 1 \text{ GeV}^2$ and $x_{\text{Bj}} = 10^{-5}$ at $Q^2 = 2 \text{ GeV}^2$ [34]. These very low- Q^2 and low- x_{Bj} data are mostly not included in the present HHT analysis. This analysis is based on the DGLAP formalism which is not expected to work for Q^2 as low as 1 GeV^2 . The necessary Q_{min}^2 cut limits the range of the fitted data in x_{Bj} such that the data used here just touch the predicted critical line.

Results on F_2 and F_L are presented for selected values of the energy at the photon–proton vertex, W , to separate out the low- x_{Bj} regime of the data ($x_{\text{Bj}} = Q^2/(W^2 + Q^2)$) and to compare to the predictions of GBW. Figures 12 and 13 show extractions² together with the corresponding predictions for F_2 and F_L for the high-precision NC e^+p data for HHT and HERAPDF2.0 at NNLO and NLO, respectively. The data used here are limited to $Q^2 \geq Q_{\text{min}}^2 = 3.5 \text{ GeV}^2$ and approach the critical regime of x_{Bj} only for $W = 276 \text{ GeV}$. The predictions of GBW, also shown in Figs. 12 and 13, agree reasonably well with the F_2 predictions of HHT up to Q^2 of about 10 GeV^2 at this highest W value, the only W value where HHT and HERAPDF2.0 differ significantly. The values of $F_2^{\text{extracted}}$ are significantly larger for HHT in this low- x_{Bj} regime than for HERAPDF2.0 and they agree better with the corresponding predictions. This is true for fits at NNLO and at NLO. In both cases, it is caused by significantly larger values of F_L , since Eq. 1 implies that F_2 must also increase.

For Figs. 12 and 13, all predictions from HHT and HERAPDF2.0 were extrapolated down to $Q^2 = 1.2 \text{ GeV}^2$, a value below the starting scale, for which the predictions of HHT NNLO nevertheless still describe the reduced cross sections quite well, see Fig. 7. The predictions from GBW are expected to be particularly relevant in this regime while the pQCD evolution on which HHT and HERAPDF2.0 are based is expected to start to break down. This is demonstrated by the results on F_L . The extractions and predictions differ substantially between NNLO and NLO for Q^2 below 10 GeV^2 . At NLO, the predicted F_L values become negative for all three W values as Q^2 approaches 1 GeV^2 for both HERAPDF2.0 and HHT. This is unphysical. At NNLO, all predicted F_L values start to increase as Q^2 approaches 1 GeV^2 . For HHT NNLO, this increase is dramatic.

Figures 12 and 13 also demonstrate that values of $F_L^{\text{extracted}}$ cannot be considered measurements. Even though the predictions of HHT and HERAPDF2.0 differ significantly below 100 GeV^2 , the extractions seem to simply reflect those predictions. This demonstrates the importance of direct F_L measurements.

Figure 14 shows predictions for F_L from HHT and HERAPDF2.0 at both NNLO and NLO for $W = 232 \text{ GeV}$ together with a prediction from GBW. The plot also contains measured values down to Q^2 of almost 1 GeV^2 published by the H1 collaboration [15]. The statistical accuracy

²Extracted values $F_L^{\text{extracted}}$ are calculated similarly to the values of $F_2^{\text{extracted}}$, see Eq. 5.

of these data is limited, but the strong upturn of F_L predicted by HHT NNLO is not observed. The data confirm the downward trend of the F_L values measured for the full W range shown in Fig. 11. Colour-dipole motivated models [29,34] predict that F_L becomes similar for different values of W at low Q^2 . The measured values of F_L shown in Figs. 11 and 14 are compatible with this.

The strong difference between F_L predictions from HHT NNLO and NLO, together with the HHT NNLO prediction of a strong upturn of F_L as Q^2 approaches 1 GeV^2 indicate that the current simple higher-twist correction to the perturbative DGLAP evolution alone cannot completely describe the physics involved, even though the reduced cross sections are described quite well by this *ansatz*.

8 Conclusions

The addition of a twist-4 term to the description of the longitudinal structure function F_L significantly improved the quality of pQCD fits within the DGLAP framework to HERA data. In particular, the description of cross sections at low Q^2 and low x_{Bj} was improved. The Q^2 range of the fits was extended down to $Q^2 = 2.0 \text{ GeV}^2$ and the cross-section data could be well described down to $Q^2 = 1.2 \text{ GeV}^2$ by extrapolations. The addition of a higher-twist term to the structure function F_2 has no effect. This confirms the expectation that the influence of higher-twist effects cancels for longitudinally and transversely polarised photons in F_2 .

The recombination of gluons is part of the higher-twist formalism. This can be seen as a mechanism of saturation. The strong influence of such a higher-twist term can be seen as the first hint for the onset of saturation in the HERA data at low Q^2 and low x_{Bj} . The predictions of HHT NNLO for F_L become very high for Q^2 below 3.5 GeV^2 and disagree with the data. This indicates that the pQCD description is breaking down and further mechanisms are needed for a consistent description of the data at the lowest x_{Bj} and Q^2 .

9 Acknowledgements

We are grateful to our ZEUS colleagues who supported this work. We thank our funding agencies, especially the Alexander von Humboldt foundation, for financial support and DESY for the hospitality extended to the non-DESY authors. We also thank K. Golec-Biernat for discussions and providing the predictions of the GBW model.

References

- [1] A. M. Cooper-Sarkar and R. Devenish, *Deep Inelastic Scattering* (Oxford University Press, (2011)).
- [2] F. Aaron *et al.* [ZEUS and H1 Collaboration], JHEP **1001**, 109 (2010), [arXiv:0911.0884].
- [3] H. Abramowicz *et al.* [ZEUS and H1 Collaboration], Eur. Phys. J. C **75**, 580 (2015), [arXiv:1506.06042].
- [4] V. Gribov and L. Lipatov, Sov. J. Nucl. Phys. **15**, 438 (1972).
- [5] V. Gribov and L. Lipatov, Sov. J. Nucl. Phys. **15**, 675 (1972).
- [6] L. Lipatov, Sov. J. Nucl. Phys. **20**, 94 (1975).
- [7] Y. Dokshitzer, Sov. Phys. JETP **46**, 641 (1977).
- [8] G. Altarelli and G. Parisi, Nucl. Phys. B **126**, 298 (1977).
- [9] E. Kuraev, L. Lipatov, and F. Fadin, Sov. Phys. JETP **45**, 199 (1977).
- [10] J. Bartels, K. Golec-Biernat, and K. Peters, Eur. Phys. J. C **71**, 121 (2000), [hep-ph/0003042v4].
- [11] J. Bartels, K. Golec-Biernat, and H. Kowalski, Phys. Rev. D **66**, 014001 (2002), [hep-ph/0203258].
- [12] F. Caola, S. Forte, and J. Rojo, Phys. Lett. B **686**, 127 (2009), [arXiv:0910.3143].
- [13] J. Rojo (2015), [arXiv:1508.07731].
- [14] A. M. Cooper-Sarkar *et al.*, Z. Phys. C **39**, 281 (1988).
- [15] V. Andreev *et al.* [H1 Collaboration], Eur. Phys. J. C **73**, 2814 (2013), [arXiv:1312.4821].
- [16] H. Abramowicz *et al.* [ZEUS Collaboration], Phys. Rev. D **90**, 072002 (2014), [arXiv:1404.6376].
- [17] S. Alekhin, J. Blumlein, and S. Moch, Phys. Rev. D **86**, 054009 (2012), [arXiv:1202.2281].
- [18] L. Motyka, M. Sadzikowski, and W. Slominski, Phys. Rev. D **86**, 111501 (2012), [arXiv:1203.5461].
- [19] H. Abramowicz *et al.* [ZEUS Collaboration] Phys. Rev. D **93**, 092002 (2016), [arXiv:1603.09628].
- [20] S. Alekhin *et al.* (2014), [arXiv:1410.4412].
- [21] R. S. Thorne and R. G. Roberts, Phys. Rev. D **57**, 6871 (1998), [hep-ph/9709442].
- [22] R. S. Thorne, Phys. Rev. D **73**, 054019 (2006), [hep-ph/0601245].

- [23] R. S. Thorne, Phys. Rev. D **86**, 074017 (2012), [arXiv:1201.6180].
- [24] A. D. Martin, W. J. Stirling, R. S. Thorne, and G. Watt, Eur. Phys. J. C **63**, 189 (2009), [arXiv:0901.0002].
- [25] L. A. Harland-Lang, A. D. Martin, P. Motylinski, and R. S. Thorne, Eur. Phys. J. C **75** (2015), [arXiv:1412.3989].
- [26] L. A. Harland-Lang, A. D. Martin, P. Motylinski, and R. S. Thorne (2016), [arXiv:1601.03413].
- [27] M. Cacciari, M. Greco, and P. Nason, JHEP **9805**, 007 (1998), [hep-ph/9803400].
- [28] S. Forte, E. Laenen, P. Nason, and J. Rojo, Nucl. Phys. B **834**, 116 (2010), [arXiv:1001.2312].
- [29] A. D. Martin, W. J. Stirling, and R. S. Thorne, Phys. Lett. B **635**, 305 (2006), [hep-ph/0601247].
- [30] A. Caldwell (2016), [arXiv:1601.04472v1].
- [31] I. Balitsky, Nucl. Phys. B **463**, 99 (1996), [hep-ph/9509348].
- [32] Y. Kovchegov, Phys. Rev. D **60**, 034008 (1999), [hep-ph/9901281].
- [33] J. L. Albacete *et al.*, Eur. Phys. J. C **71**, 1705(2011), [arXiv:1012.4408].
- [34] K. Golec-Biernat and M. Wüsthoff, Phys. Rev. D **59**, 014017 (1998), [hep-ph/9807513].

| Fit at | with $Q_{\min}^2 = 3.5 \text{ GeV}^2$ | HERAPDF2.0 | HHT | $A_L^{\text{HT}}/\text{GeV}^2$ |
|--------|---|------------|-----------|--------------------------------|
| NNLO | χ^2/ndof | 1363/1131 | 1316/1130 | 5.5 ± 0.6 |
| | χ^2/ndp for NC e^+p : $Q^2 \geq Q_{\min}^2$ | 451/377 | 422/377 | |
| | χ^2/ndp for NC e^+p : $2.0 \text{ GeV}^2 \leq Q^2 < Q_{\min}^2$ | 41/25 | 32/25 | |
| NLO | χ^2/ndof | 1356/1131 | 1329/1130 | 4.2 ± 0.7 |
| | χ^2/ndp for NC e^+p : $Q^2 \geq Q_{\min}^2$ | 447/377 | 431/377 | |
| | χ^2/ndp for NC e^+p : $2.0 \text{ GeV}^2 \leq Q^2 < Q_{\min}^2$ | 46/25 | 46/25 | |

Table 1: Table of χ^2 values for the HHT fit compared to the equivalent HERAPDF2.0 fit, both with $Q_{\min}^2 = 3.5 \text{ GeV}^2$. Also listed are the partial $\chi^2/(\text{number of data points, ndp})$ values of the fits for the high-precision NC e^+p data at $\sqrt{s} = 318 \text{ GeV}$ for $Q^2 \geq Q_{\min}^2$. The final row for each fit lists the χ^2/ndp for its predictions for Q^2 below the fitted region down to 2.0 GeV^2 . In addition, the higher-twist parameters for HHT fits are given.

| Fit at | with $Q_{\min}^2 = 2.0 \text{ GeV}^2$ | HERAPDF2.0 | HHT | $A_L^{\text{HT}}/\text{GeV}^2$ |
|--------|---|------------|-----------|--------------------------------|
| NNLO | χ^2/ndof | 1437/1171 | 1381/1170 | 5.2 ± 0.7 |
| | χ^2/ndp for NC e^+p : $Q^2 \geq Q_{\min}^2$ | 486/402 | 457/402 | |
| | χ^2/ndp NC e^+p : $Q_{\min}^2 \leq Q^2 < 3.5 \text{ GeV}^2$ | 31/25 | 26/25 | |
| NLO | χ^2/ndof | 1433/1171 | 1398/1170 | 4.0 ± 0.6 |
| | χ^2/ndp for NC e^+p : $Q^2 \geq Q_{\min}^2$ | 487/402 | 466/402 | |
| | χ^2/ndp NC e^+p : $Q_{\min}^2 \leq Q^2 < 3.5 \text{ GeV}^2$ | 40/25 | 31/25 | |

Table 2: Table of χ^2 values for the HHT fit compared to the equivalent HERAPDF2.0 fit, both with $Q_{\min}^2 = 2.0 \text{ GeV}^2$. Also listed are the partial χ^2/ndp values of the fits for the high-precision NC e^+p data at $\sqrt{s} = 318 \text{ GeV}$ for $Q^2 \geq Q_{\min}^2$. The final row for each fit lists the partial χ^2/ndp of the fit for data points with $2.0 \leq Q^2 < 3.5 \text{ GeV}^2$. In addition, the higher-twist parameters for HHT fits are given.

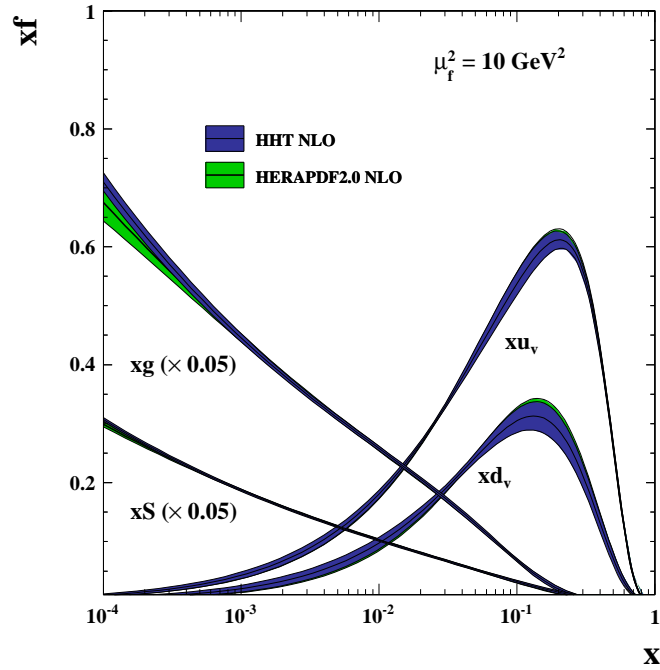
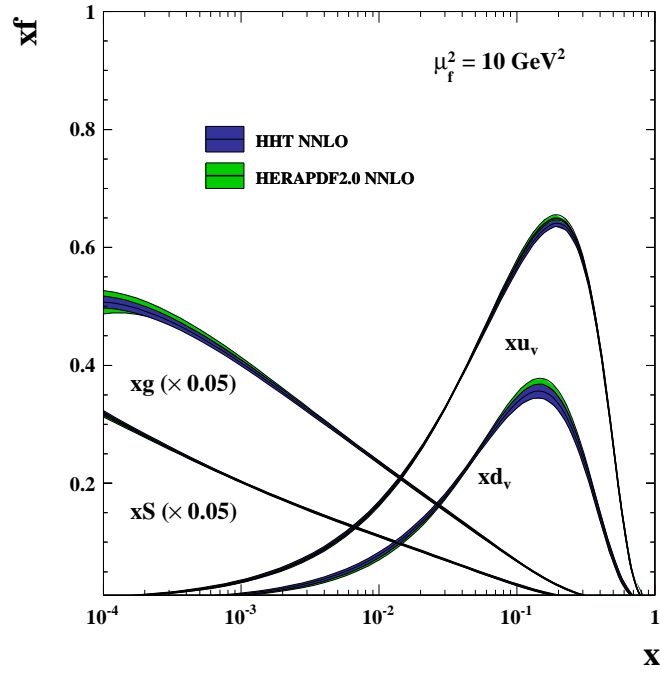


Figure 1: The HHT parton distribution functions, xu_v , xd_v , xS and xg , at the scale $\mu_f^2 = 10 \text{ GeV}^2$ compared to the PDFs from HERAPDF2.0 at NNLO (top) and NLO (bottom). The gluon and sea distributions are scaled down by a factor 20. The bands represent the experimental, i.e. fit, uncertainties.

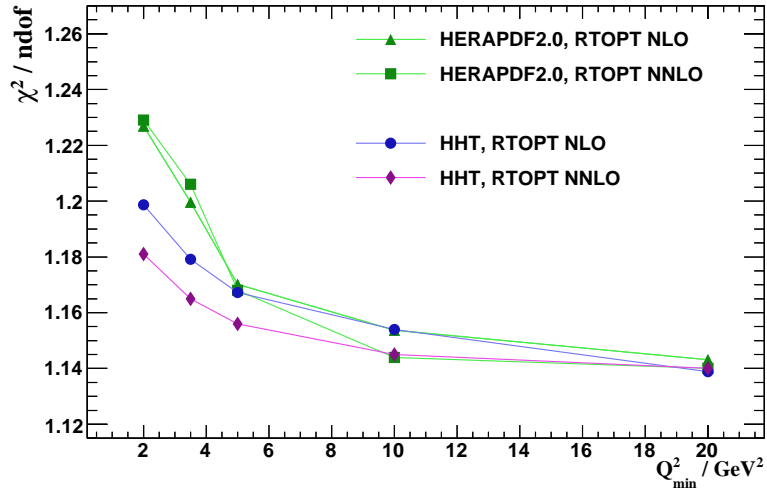


Figure 2: The χ^2/ndof versus Q_{\min}^2 for HHT and HERAPDF2.0 fits at NNLO and NLO.

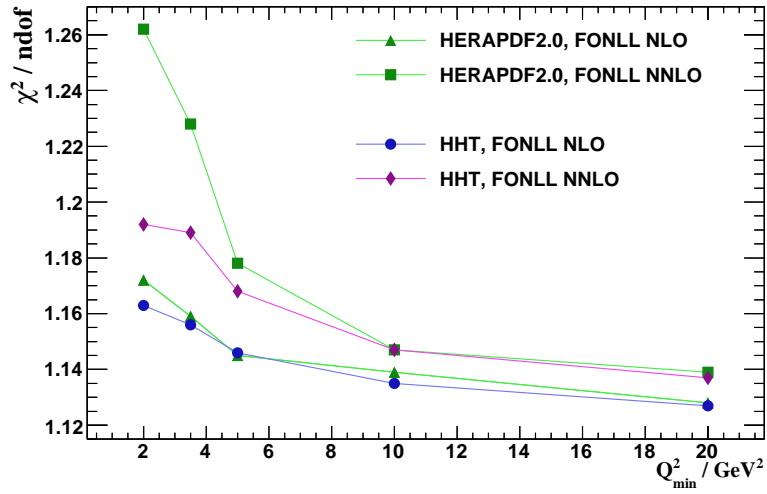


Figure 3: The χ^2/ndof versus Q_{\min}^2 for HHT and HERAPDF2.0 fits at NNLO and NLO using the FONLL heavy-flavour scheme instead of the default RTOPT scheme.

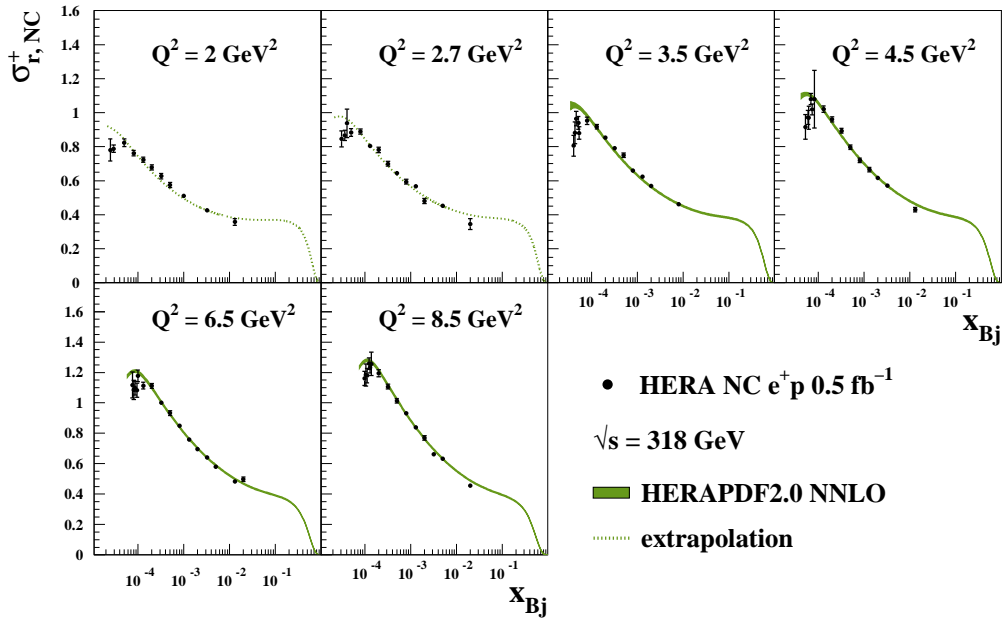
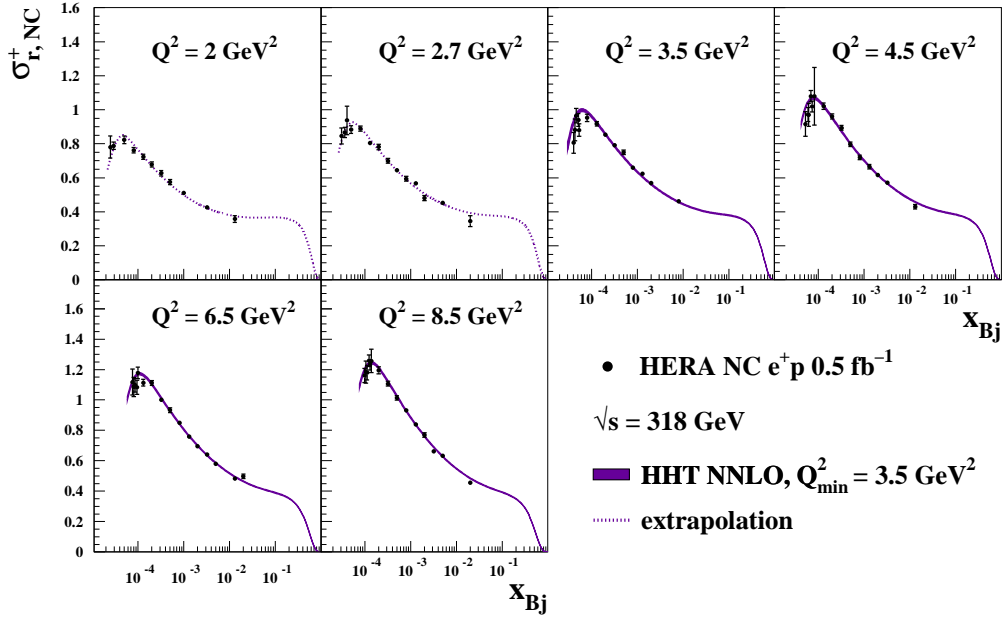


Figure 4: The predictions of HHT NNLO (top) and HERAPDF2.0 NNLO (bottom), both with $Q_{\min}^2 = 3.5 \text{ GeV}^2$, compared to the HERA measurements of σ_r . The bands represent the experimental, i.e. fit, uncertainties. Extrapolations are indicated as dotted lines.

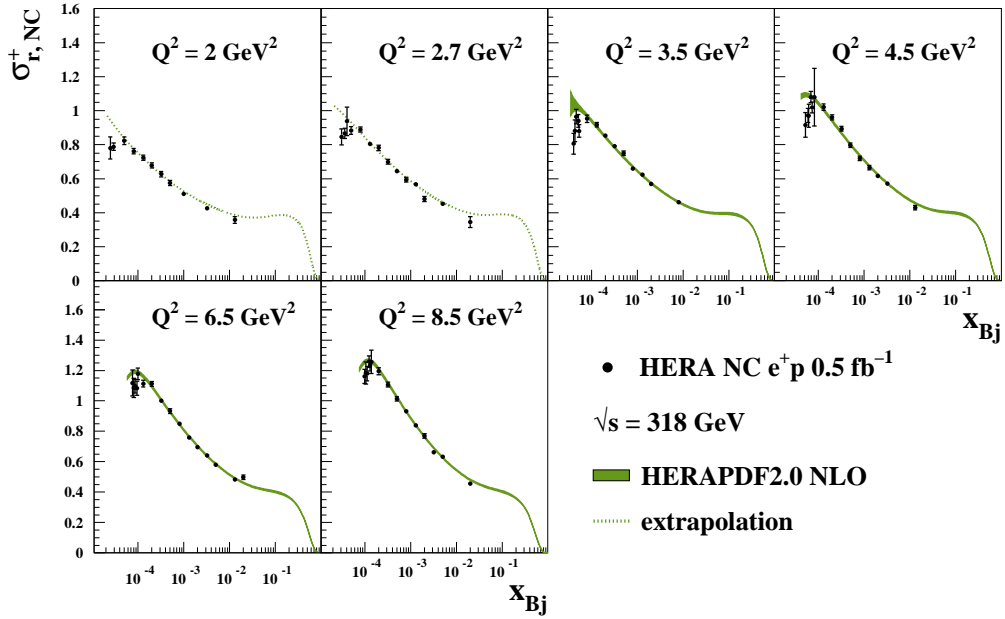
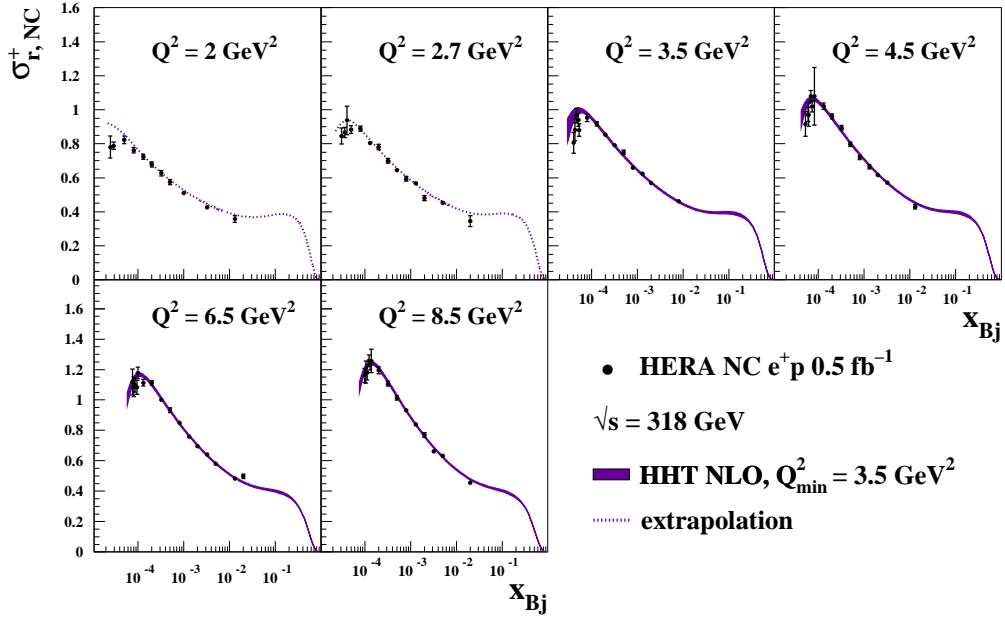


Figure 5: The predictions of HHT NLO (top) and HERAPDF2.0 NLO (bottom), both with $Q_{\min}^2 = 3.5 \text{ GeV}^2$, compared to the HERA measurements of σ_r . The bands represent the experimental, i.e. fit, uncertainties. Extrapolations are indicated as dotted lines.

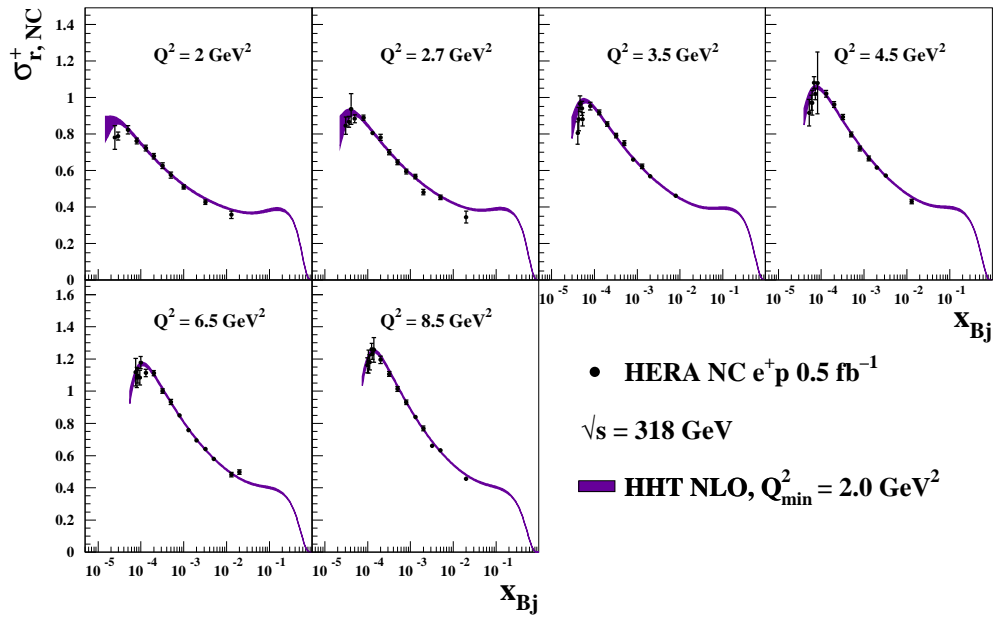
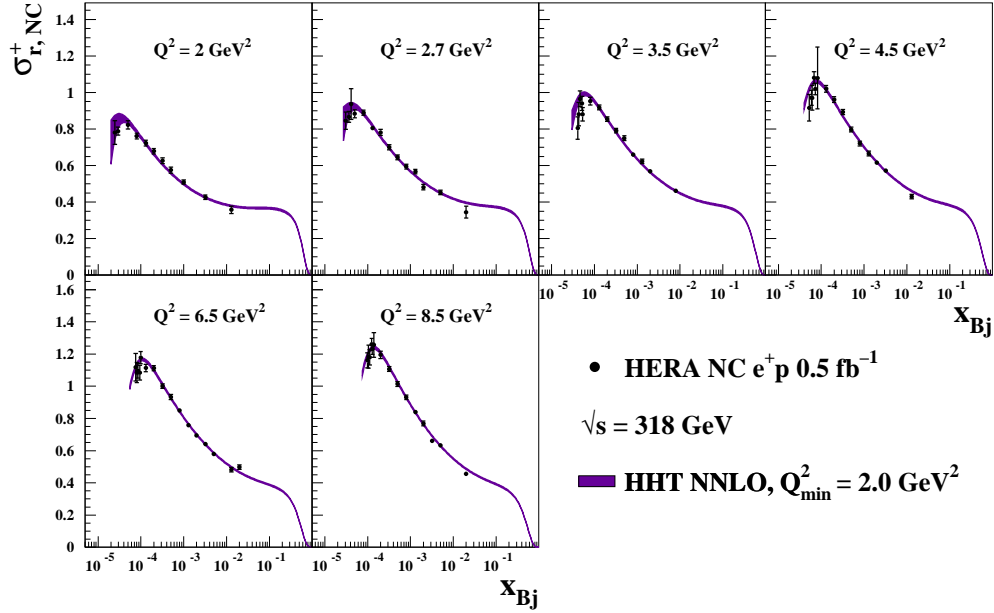


Figure 6: The predictions of HHT NNLO (top) and HHT NLO (bottom) with $Q_{\min}^2 = 2.0 \text{ GeV}^2$ compared to the HERA measurements of σ_r . The bands represent the experimental, i.e. fit, uncertainties.

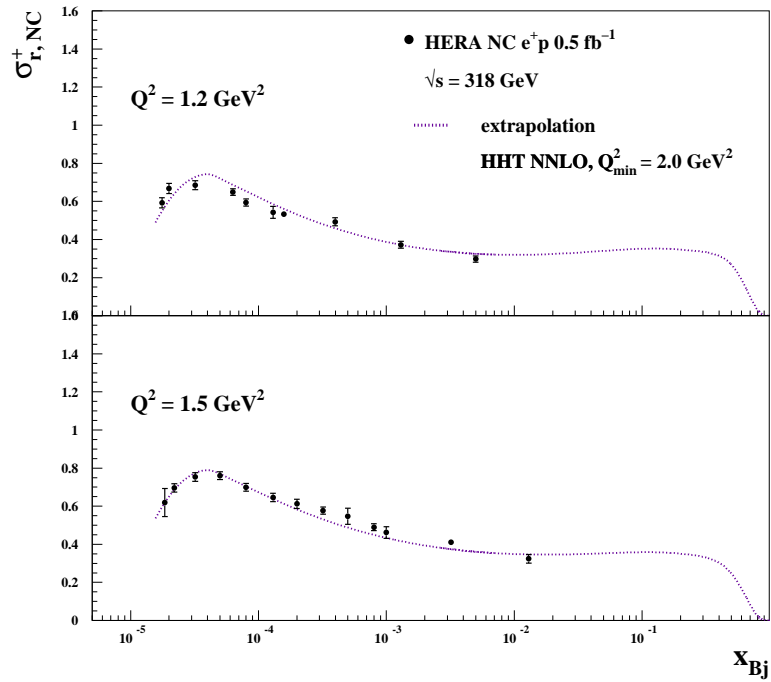
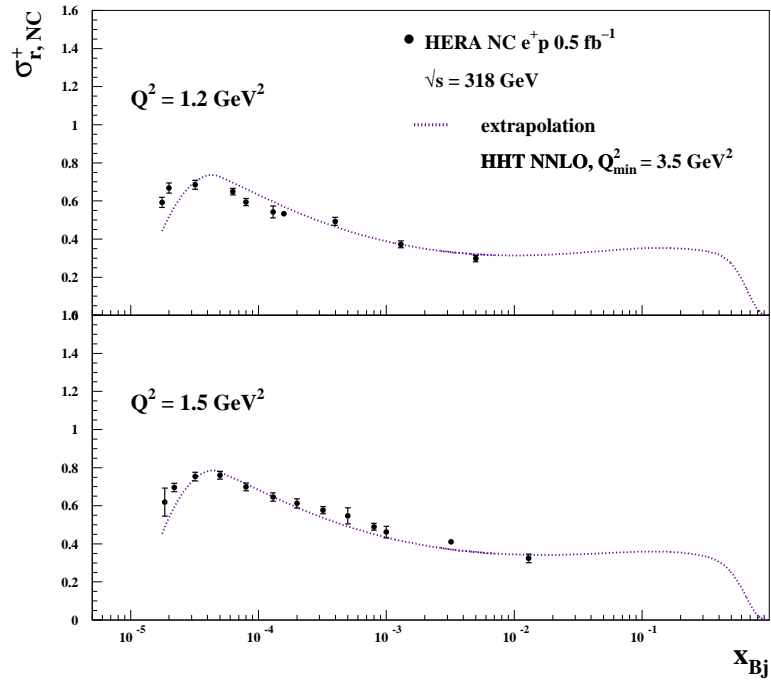


Figure 7: The extrapolated predictions of HHT NNLO with with $Q_{\min}^2 = 3.5 \text{ GeV}^2$ (top) and with $Q_{\min}^2 = 2.0 \text{ GeV}^2$ (bottom) compared to the HERA NC e^+p measurements of σ_r at Q^2 of 1.2 and 1.5 GeV^2 .

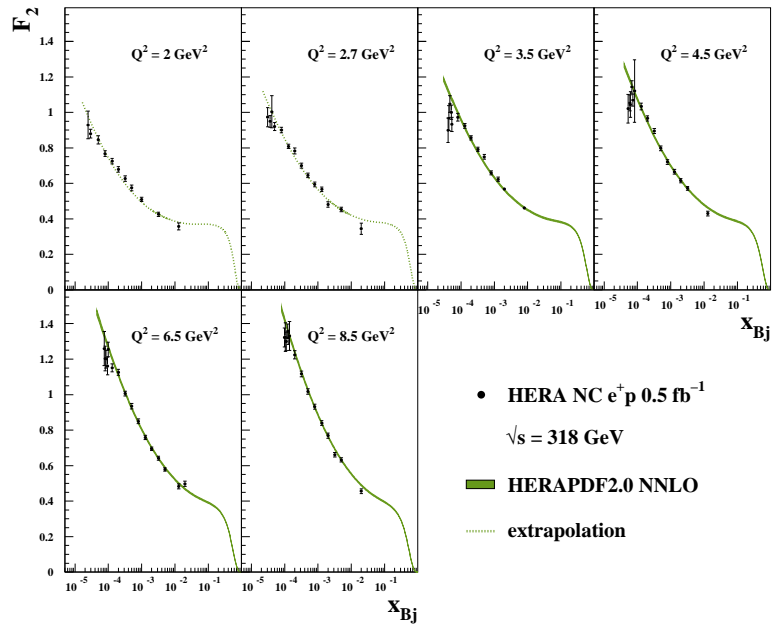
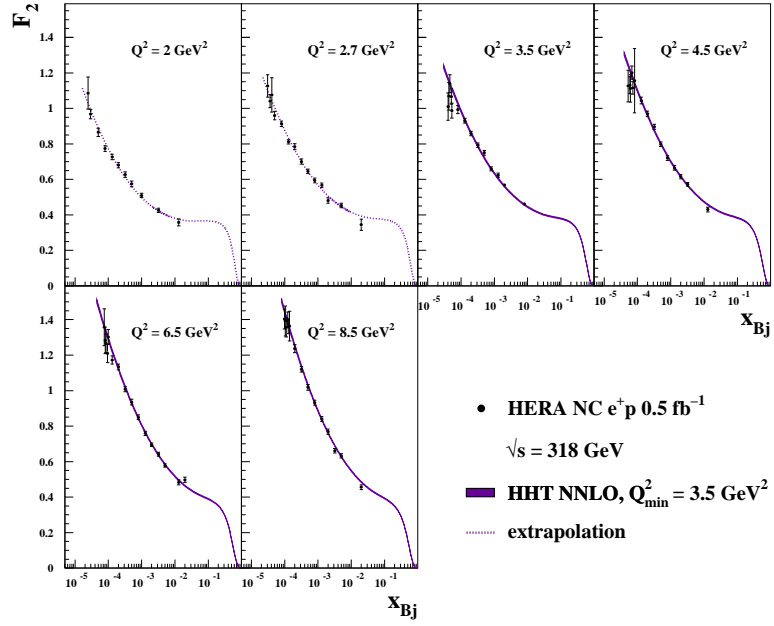


Figure 8: The predictions of HHT NNLO (top) and HERAPDF2.0 NNLO (bottom), both with $Q_{\min}^2 = 3.5 \text{ GeV}^2$, compared to extracted values $F_2^{\text{extracted}}$. The bands represent the experimental, i.e. fit, uncertainties. Extrapolations are indicated as dotted lines.

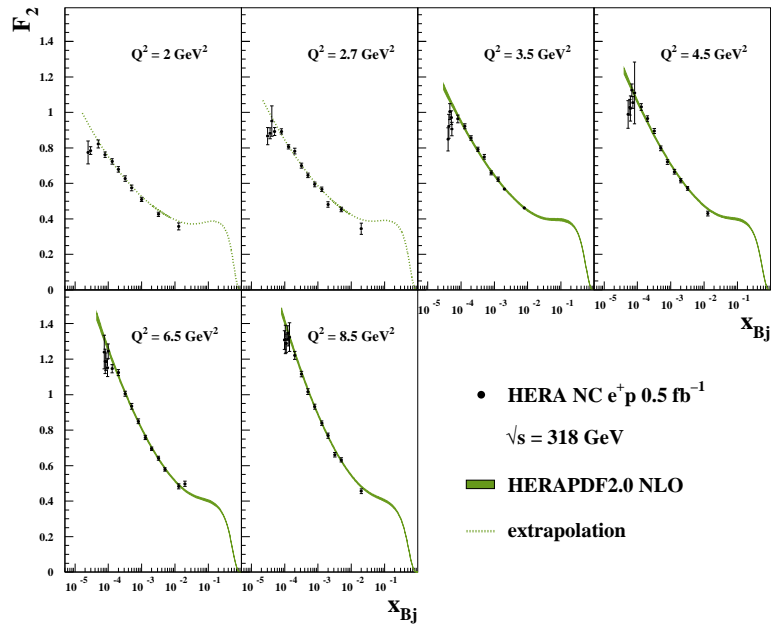
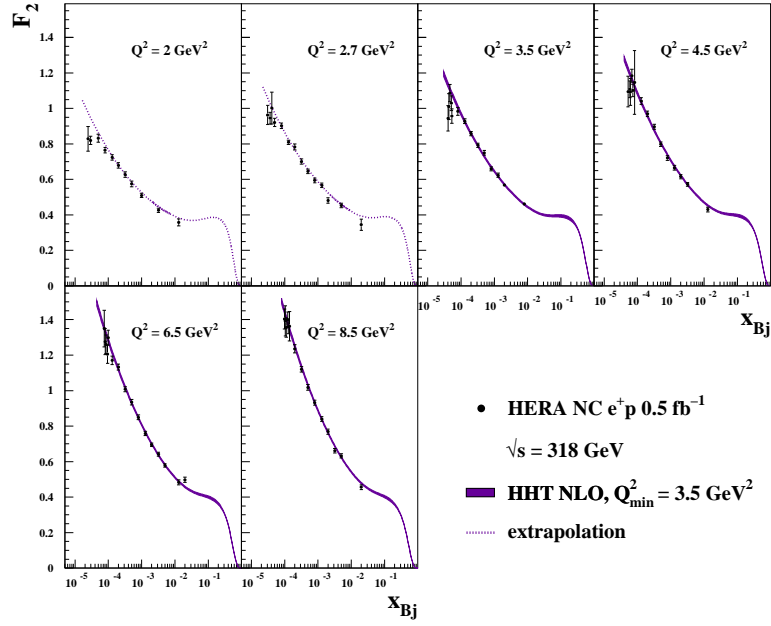


Figure 9: The predictions of HHT NLO (top) and HERAPDF2.0 NLO (bottom) both with $Q_{\min}^2 = 3.5 \text{ GeV}^2$, compared to extracted values $F_2^{\text{extracted}}$. The bands represent the experimental, i.e. fit, uncertainties. Extrapolations are indicated as dotted lines.

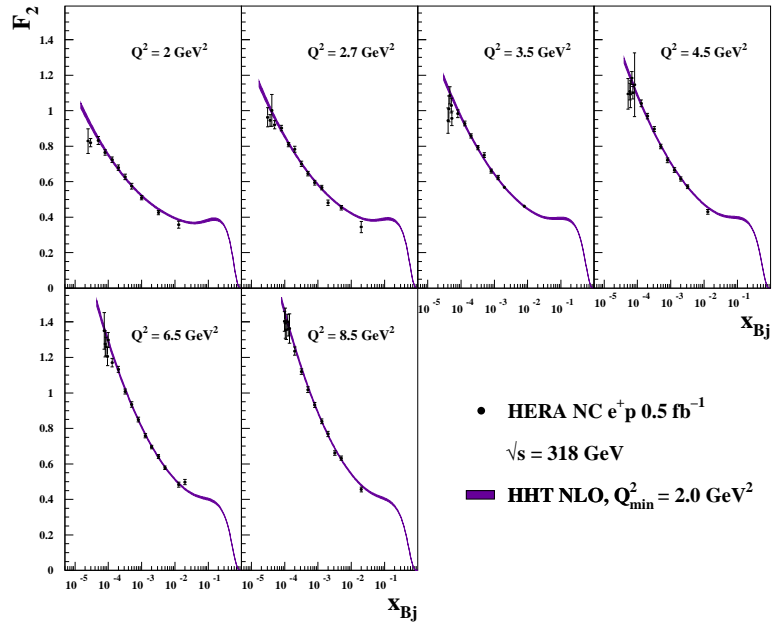
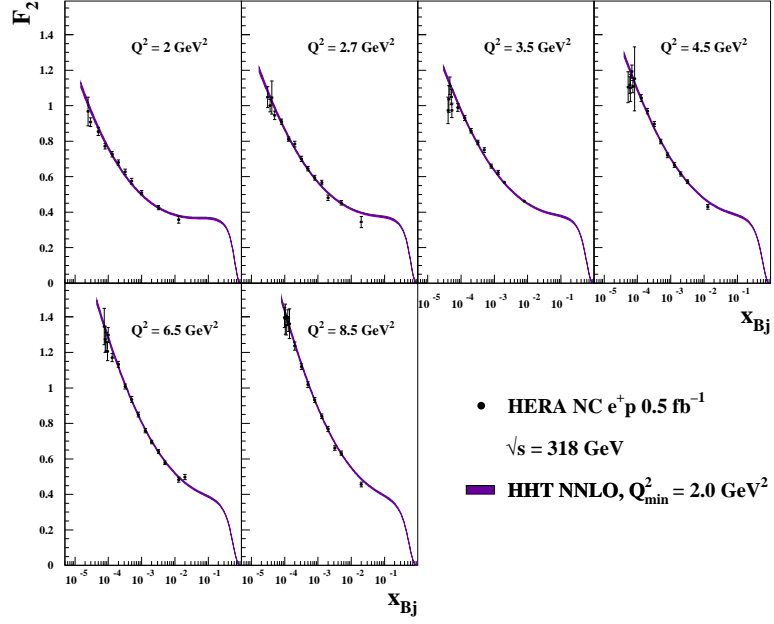


Figure 10: The predictions of HHT NNLO (top) and HHT NLO (bottom) with $Q_{\min}^2 = 2.0 \text{ GeV}^2$ compared to extracted values $F_2^{\text{extracted}}$. The bands represent the experimental, i.e. fit, uncertainties.

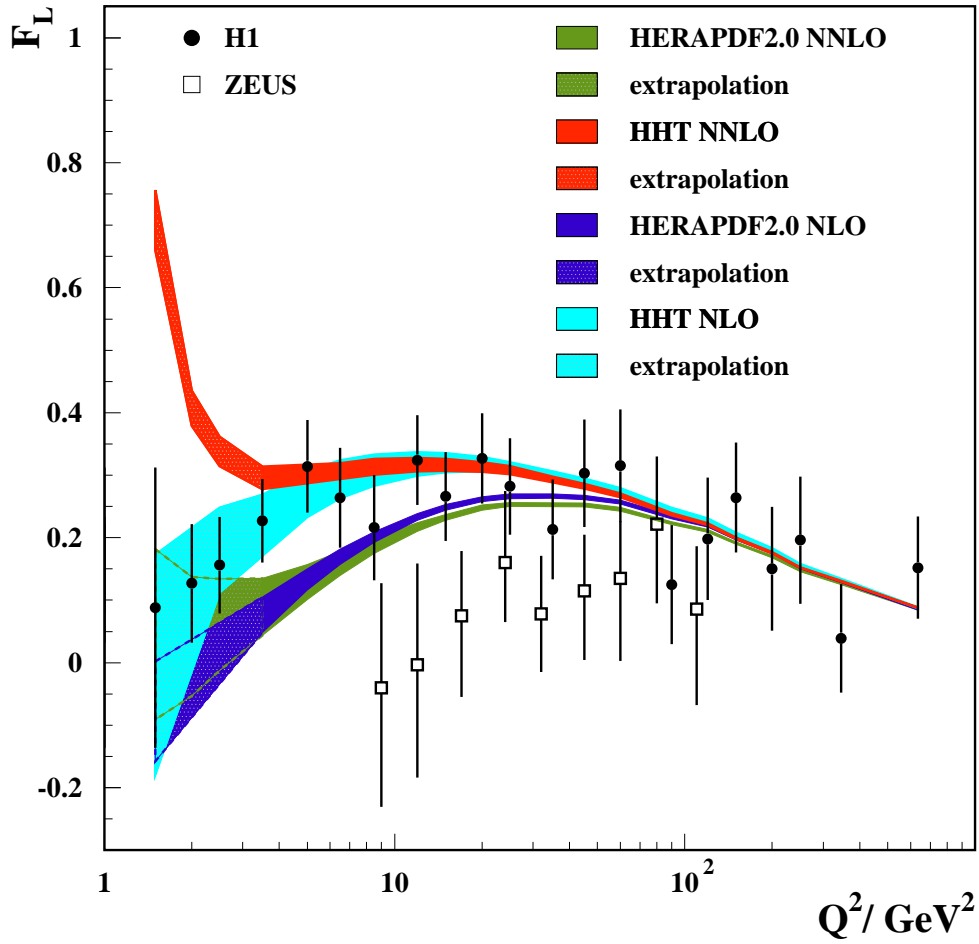


Figure 11: The predictions for F_L from HHT and HERAPDF2.0, both with $Q_{\min}^2 = 3.5 \text{ GeV}^2$, compared to the separate direct measurements published by the H1 and ZEUS collaborations. The bands represent the experimental, i.e. fit, uncertainties on the predictions. Hatched bands represent extrapolations.

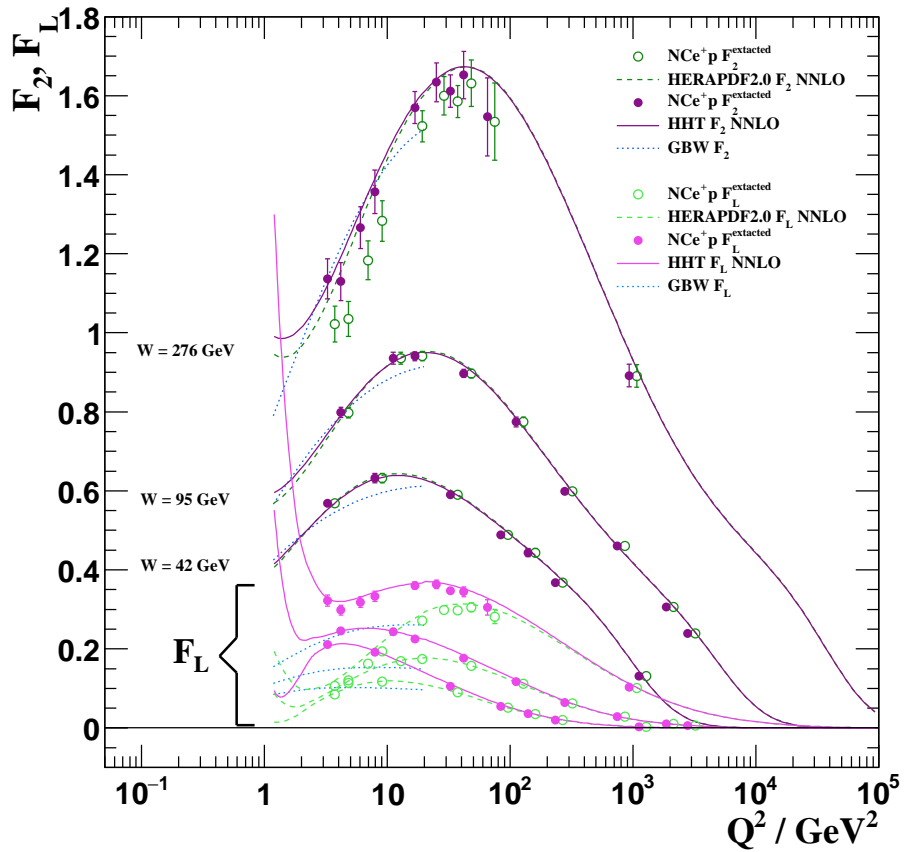


Figure 12: The $F_2^{\text{extracted}}$ and $F_L^{\text{extracted}}$ values as extracted from HHT NNLO and HERAPDF2.0 NNLO together with the corresponding predictions from HHT NNLO and HERAPDF2.0 NNLO for three selected values of W . Also shown are predictions from the GBW model.

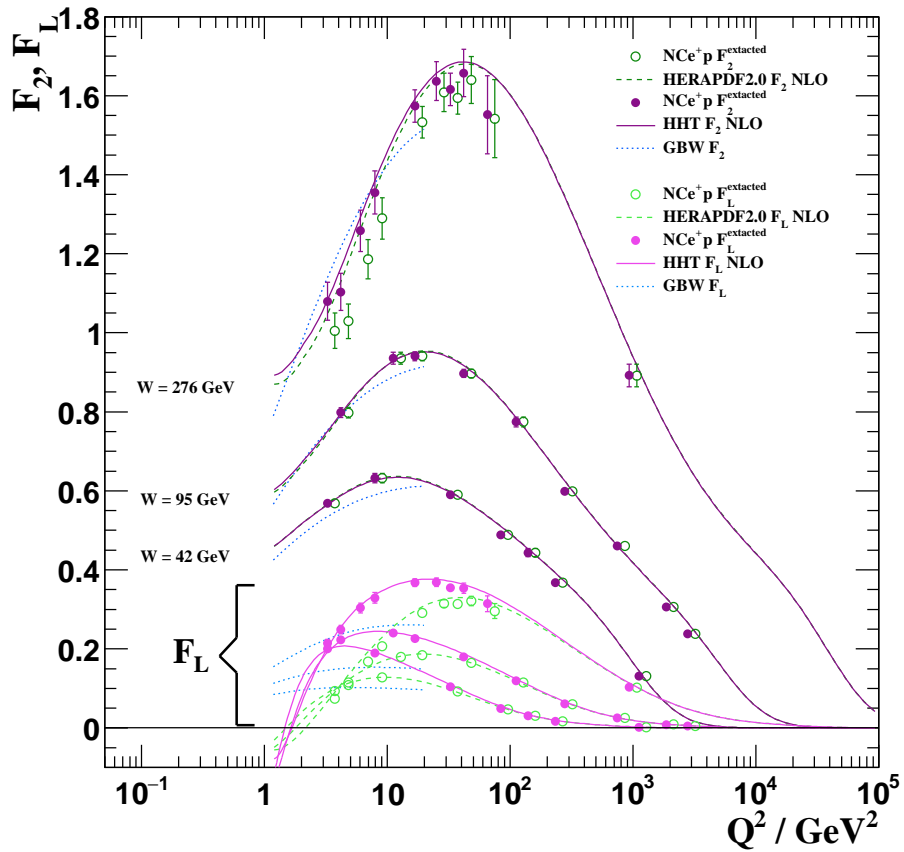


Figure 13: The $F_2^{\text{extracted}}$ and $F_L^{\text{extracted}}$ values as extracted from HHT NLO and HERAPDF2.0 NLO together with the corresponding predictions from HHT NLO and HERAPDF2.0 NLO for three selected values of W . Also shown are predictions from the GBW model.

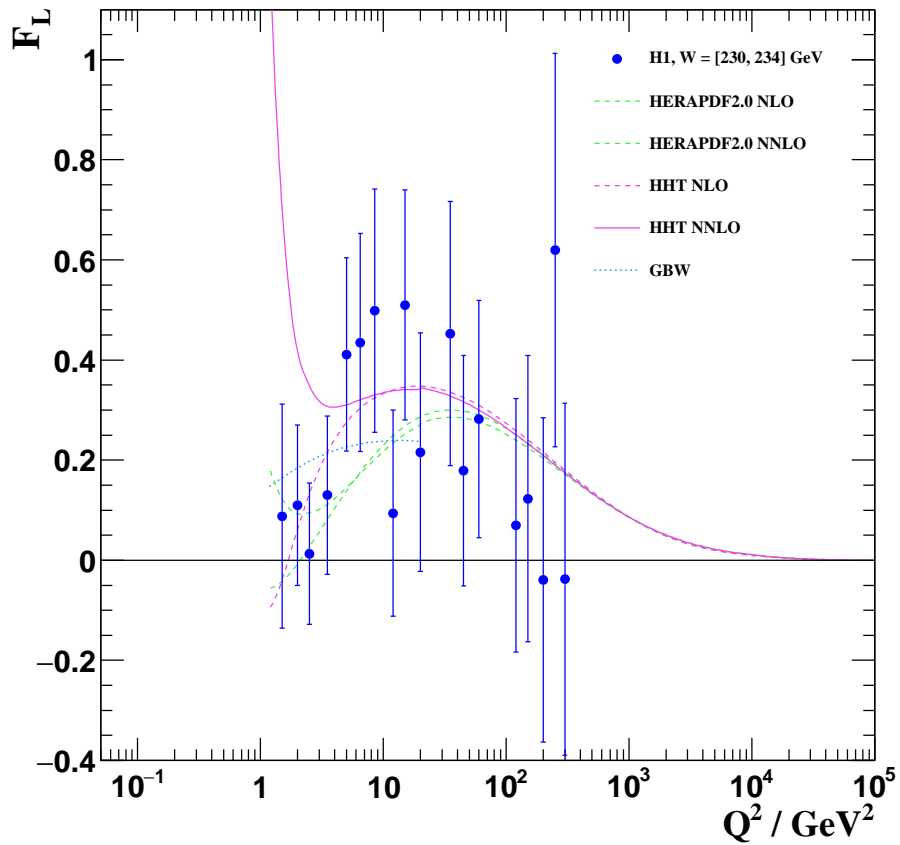


Figure 14: The predictions from HHT and HERAPDF2.0 at NNLO and NLO for $W = 232$ GeV, together with direct measurements of F_L published by the H1 collaboration for W between 230 and 234 GeV. Also shown is the prediction from the GBW model.